





## Conventional photon blockade with a three-wave mixing

Y. H. Zhou <sup>1</sup>, X. Y. Zhang <sup>2</sup>, Q. C. Wu,<sup>1</sup> B. L. Ye,<sup>1</sup> Zhi-Qiang Zhang <sup>3</sup>, D. D. Zou,<sup>4</sup> H. Z. Shen,<sup>5,\*</sup> and Chui-Ping Yang <sup>1,†</sup>

<sup>1</sup>Quantum Information Research Center, Shangrao Normal University, Shangrao 334001, China

<sup>2</sup>Department of Physics, Dalian Maritime University, Dalian 116026, China

<sup>3</sup>General Education Centre, Zhengzhou Business University, Gongyi Henan 451200, China

<sup>4</sup>College of Physics and Electronic Information, Shangrao Normal University, Shangrao 334001, China

<sup>5</sup>Center for Quantum Sciences and School of Physics, Northeast Normal University, Changchun 130024, China



(Received 5 August 2019; revised 13 July 2020; accepted 17 August 2020; published 10 September 2020)

The conventional photon blockade is studied in a three-wave-mixing system. The analytic conditions for realizing the photon blockade are obtained by analyzing the eigenvalues of the system Hamiltonian, which is expanded by an effective single excited space for the high-frequency mode. The numerical results are calculated by solving the master equation in a truncated Fock space, which agrees well with the analytic conditions. Different from the other schemes of the conventional photon blockade, photon antibunching can be realized in the three modes of the three-wave-mixing system simultaneously due to the nature of the system.

DOI: [10.1103/PhysRevA.102.033713](https://doi.org/10.1103/PhysRevA.102.033713)

### I. INTRODUCTION

The control and manipulation of a single photon have become an active area of research in modern quantum optics and quantum information processing in recent years [1–13]. To this end, the study of a single-photon source has become a conspicuous focus in quantum physics, which can be realized by the photon blockade (PB) effect. The PB effect is a phenomenon that a single photon in a nonlinear cavity blocks the transmission of a second one [14–20]. The photon blockade yields antibunching, and we should find the systems to produce sub-Poissonian light when it is driven by a classical light field. Since the photon blockade was proposed, this nonclassical effect has attracted significant experimental and theoretical attention due to the applications in information and communication technology. In the process of PB development, two main physical mechanisms are discovered to realize this effect: The PB enabled by the energy-level splitting due to the nonlinearity of the system is known as a conventional phonon blockade (CPB) [21]. The PB enabled by the quantum interference is named as an unconventional photon blockade [22–24], which has been recently observed experimentally [25,26]. In this paper, we are only concerned with the CPB, which was observed for the first time experimentally in the system of an optical cavity coupled to a single trapped atom [21]. After that, different experimental groups observed the CPB in different systems, including a quantum dot in a photonic crystal system [27] and circuit cavity quantum electrodynamics systems [28,29]. In the meanwhile, the studies of the CPB have also advanced using different systems [30–36]. In addition to the single-photon sources, the PB has other applications in quantum optics and quantum information

processing, such as the realizing of single-photon transistors [37], interferometers [38], and quantum optical diodes [36]. Recently, the antiblockade [39–41] and PB in non-Markovian systems [17] were also studied.

In this paper, we study the CPB based on a three-wave-mixing system, where the three-wave mixing mediates the conversion of a photon with high frequency into two photons with different low frequencies. The analytical conditions for the CPB are obtained by analyzing the eigenvalues of the system Hamiltonian. We compare the numerical results with the analytical conditions and find they are in good agreement, which confirms the analytic conditions and the corresponding analysis. The contribution of the present paper can be summarized as follows.

(i) A system is proposed to realize the CPB, which can act as a candidate to realize single-photon sources.

(ii) The three-wave mixing provides the present paper with the feature that the CPB can be obtained in the three modes with different output frequencies.

The remainder of this paper is organized as follows. In Sec. II, we introduce the physical model. In Sec. III, we illustrate the analytical conditions for the photon blockade and the physical mechanism based on the three-wave mixing. In Sec. IV, we show the numerical results and compare them with the analytical conditions for the photon blockade. We also investigate the photon blockade effect with nonzero temperature. Discussion and conclusions are given in Sec. V.

### II. PHYSICAL MODEL

In this paper, we investigate the CPB in a three-wave-mixing system. The three-wave-mixing process includes a high-frequency mode  $a$  with frequency  $\omega_a$  and two low-frequency modes  $b$  and  $c$  with frequencies  $\omega_b$  and  $\omega_c$ , respectively. The three-wave-mixing process can be described

\*Corresponding author: shenhz458@nenu.edu.cn

†Corresponding author: yangcp@hznpu.edu.cn

by the following Hamiltonian [42,43]:

$$\hat{H}_0 = \omega_a \hat{a}^\dagger \hat{a} + \omega_b \hat{b}^\dagger \hat{b} + \omega_c \hat{c}^\dagger \hat{c} + g(\hat{a}^\dagger \hat{b} \hat{c} + \hat{c}^\dagger \hat{b}^\dagger \hat{a}), \quad (1)$$

where  $\hat{a}$ ,  $\hat{b}$ , and  $\hat{c}$  denote the annihilation operators of modes  $a$ ,  $b$ , and  $c$ , respectively. And  $g$  denotes the coefficient of the three-wave-mixing interactions. The energy conservation condition  $\omega_a = \omega_b + \omega_c$  needs to be satisfied to ensure a maximum value of  $g$ . The three-wave mixing has been studied extensively both theoretically and experimentally. In a recent experiment, the model was realized by a triply resonant microring resonator coupled by second-order optical nonlinearity with the fabricated aluminum nitride (AlN) microring structure [42].

In this paper, we drive the three modes simultaneously. In such a case, the Hamiltonian for this system reads

$$\hat{H} = \hat{H}_0 + (\varepsilon_{la} e^{-i\omega_{la}t} \hat{a}^\dagger + \varepsilon_{lb} e^{-i\omega_{lb}t} \hat{b}^\dagger + \varepsilon_{lc} e^{-i\omega_{lc}t} \hat{c}^\dagger + \text{H.c.}), \quad (2)$$

where  $\omega_{la}$ ,  $\omega_{lb}$ , and  $\omega_{lc}$  are the frequencies of weak driving fields, while  $\varepsilon_{la}$ ,  $\varepsilon_{lb}$ , and  $\varepsilon_{lc}$  are the corresponding driving strengths. In fact, the above Hamiltonian also appears in a process of down-conversion to create a single photon. However, in the process of down-conversion, it always drives the high frequency, and the photon with high frequency will be converted into two photons with low frequencies. The photon conversion is unidirectional. In our paper, the three modes are driven simultaneously, and the down-conversion and up-conversion are allowed to exist simultaneously. The photon conversion is bidirectional. And the CPB can be obtained in the three modes simultaneously.

For convenience, we would like to turn to a rotation framework subject to the operator  $\hat{U}(t) = e^{it(\omega_a \hat{a}^\dagger \hat{a} + \omega_b \hat{c}^\dagger \hat{c} + \omega_b \hat{b}^\dagger \hat{b})}$ , which leads to an effective Hamiltonian  $\hat{H}_{\text{eff}} = \hat{U} \hat{H} \hat{U}^\dagger - i\hat{U} d\hat{U}^\dagger/dt$  as

$$\begin{aligned} \hat{H}_{\text{eff}} = & \Delta_a \hat{a}^\dagger \hat{a} + \Delta_b \hat{b}^\dagger \hat{b} + \Delta_c \hat{c}^\dagger \hat{c} + g(\hat{a}^\dagger \hat{b} \hat{c} + \hat{c}^\dagger \hat{b}^\dagger \hat{a}) \\ & + [\varepsilon_{la} \hat{a}^\dagger + \varepsilon_{lb} \hat{b}^\dagger + \varepsilon_{lc} \hat{c}^\dagger + \text{H.c.}], \end{aligned} \quad (3)$$

where  $\Delta_a = \omega_a - \omega_{la}$ ,  $\Delta_b = \omega_b - \omega_{lb}$ , and  $\Delta_c = \omega_c - \omega_{lc}$ .

### III. ANALYTICAL CONDITIONS AND THE PHYSICAL MECHANISM

The Fock-state basis of the system is denoted by  $|m, n, p\rangle$  with the number  $m$  denoting the photon number in mode  $a$ ,  $n$  denoting the photon number in mode  $b$ , and  $p$  denoting the photon number in mode  $c$ . Under the weak driving limit in the steady state, we restrict to the system containing a single photon in the three modes. Here we select  $|1, 0, 0\rangle$  and  $|0, 1, 1\rangle$  to form a closed space, and the Hamiltonian can be expanded with the two bases, which can be described as a matrix form:

$$H^{(1)} = \begin{bmatrix} \Delta_a & g \\ g & \Delta_b + \Delta_c \end{bmatrix}, \quad (4)$$

where we have neglected the driving terms under the case of weak driving. Two eigenfrequencies  $\omega_+^{(1)}$  and  $\omega_-^{(1)}$  are created in the coupled system by analyzing the above matrix, which

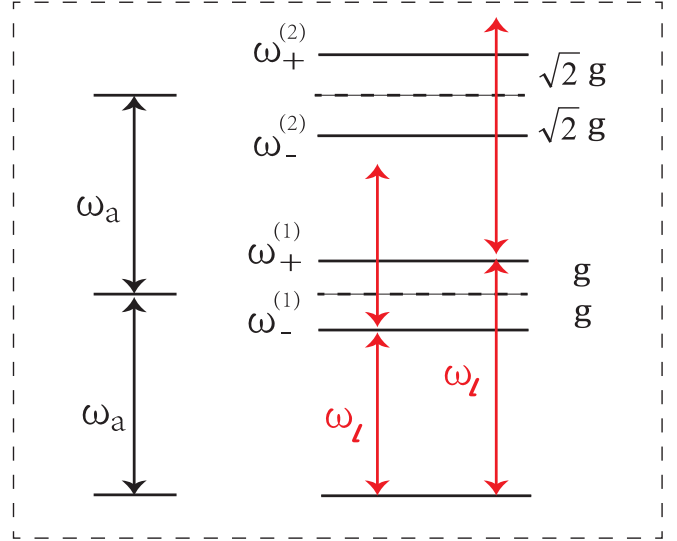


FIG. 1. Schematic energy-level diagram explaining the occurrence of the single-photon blockade by the driving field satisfying the resonance condition when  $\Delta_a = \Delta_b + \Delta_c$  is satisfied, where  $\omega_{\pm}^{(1)} = \omega_a \pm g$ ,  $\omega_{\pm}^{(2)} = 2\omega_a \pm \sqrt{6}g$ , and  $\omega^{(2)} = 2\omega_a$ .

can be written as

$$\omega_{\pm}^{(1)} = \frac{1}{2}[\Delta_a + \Delta_b + \Delta_c \pm \sqrt{4g^2 + (-\Delta_a + \Delta_b + \Delta_c)^2}], \quad (5)$$

where the superindex (1) denotes single-photon excitation for mode  $a$ . The corresponding un-normalized eigenstates are

$$\begin{aligned} |\psi_{\pm}\rangle = & \frac{\Delta_a - \Delta_b - \Delta_c \mp \sqrt{4g^2 + (-\Delta_a + \Delta_b + \Delta_c)^2}}{2g} |100\rangle \\ & + |011\rangle. \end{aligned} \quad (6)$$

The analytical conditions for the CPB can be obtained by analyzing the eigenvalues. The conditions that all the eigenvalues equal to zero can be obtained as

$$g = \pm \sqrt{\Delta_a(\Delta_b + \Delta_c)}. \quad (7)$$

The corresponding eigenstates reduce to

$$|\psi_{\pm}\rangle = \frac{\Delta_a}{g} |100\rangle + |011\rangle. \quad (8)$$

When one of the analytical conditions in Eq. (7) is met, the system will occupy the eigenstates in Eq. (8), which leads to the occurrence of the CPB. The above optimal analytical conditions for the CPB agree well with the numerical simulation, which is shown in the next subsection for studying the CPB numerically.

The physical mechanism of the CPB in the three-wave mixing system is analyzed next. The energy-level diagram of  $\hat{H}_0$  is relatively complex when Eq. (7) is satisfied, so we only analyze the case that  $\Delta_a = \Delta_b + \Delta_c$  here, which means that the conditions in Eq. (7) reduce to

$$g = \pm \Delta_a. \quad (9)$$

The energy-level diagram under the above conditions is shown in Fig. 1, where  $\omega_{\pm}^{(1)}$  is obtained by Eq. (5) without considering the driving frequency.  $\omega_{\pm}^{(2)}$  and  $\omega^{(2)}$  are the energy levels of

the system with two-photon excitation for mode  $a$ . To get the  $\omega_{\pm}^{(2)}$  and  $\omega^{(2)}$ , the Hamiltonian will be expanded with the basis  $|200\rangle$  and  $|022\rangle$ ; however, the two bases are incomplete, so we insert an intermediate state  $|111\rangle$  and the three bases can form a closed space. Under these bases, the Hamiltonian can be described as

$$\tilde{H} = \begin{bmatrix} 2\Delta_a & \sqrt{2}g & 0 \\ \sqrt{2}g & 2\Delta_a & 2g \\ 0 & 2g & 2\Delta_a \end{bmatrix}. \quad (10)$$

Three eigenfrequencies  $\omega_{\pm}^{(2)}$  and  $\omega^{(2)}$  can be obtained by solving the matrix without considering the driving frequency, which can be described as  $\omega_{\pm}^{(2)} = 2\omega_a \pm \sqrt{6}g$  and  $\omega^{(2)} = 2\omega_a$ . The superindex (2) denotes two-photon excitation for mode  $a$ .

The physical mechanism of the CPB is the anharmonic energy ladder. As shown in Fig. 1, the transition of  $0 \rightarrow \omega_{\pm}^{(1)}$  is resonant, and the transition of  $\omega_{\pm}^{(1)} \rightarrow \omega_{\pm}^{(2)}$  (or  $\omega^{(2)}$ ) is detuning. If Eq. (9) is met, the driving frequency  $\omega_l$  will equal to  $\omega_{\pm}^{(1)}$  and the single excitation resonance condition is satisfied, which leads to the single-photon probability  $p_1$  increasing dramatically. But, at the same time, the two-photon probability  $p_2$  will not change remarkably due to the detunings. Under the weak driving limit, the zero-delay-time correlation function can be expressed as  $g^{(2)}(0) \approx 2p_2/p_1^2$ . The sharp increased  $p_1$  for single excitation gives rise to an important result that  $g^{(2)}(0) \approx 0$ , and the strong single-photon blockade can be triggered. When Eq. (9) is satisfied, the output state of Eq. (8) reduces to

$$|\psi_{\pm}\rangle = \frac{1}{\sqrt{2}}(|100\rangle + |011\rangle). \quad (11)$$

The modes  $a$ ,  $b$ , and  $c$  all occupy the single-photon state, which means that the photon antibunching can be realized in the three modes of the three-wave-mixing system simultaneously.

## IV. NUMERICAL RESULTS

### A. Numerical simulation method

The statistical properties of photons will be described by the zero-delay-time second-order correlation function  $g^{(2)}(0)$ . In order to obtain  $g^{(2)}(0)$ , we need to numerically solve the master equation, which can be described as

$$\begin{aligned} \frac{\partial \hat{\rho}}{\partial t} = & -i[\hat{H}_{\text{eff}}, \rho] + \frac{\kappa_a}{2}(\bar{n}_{\text{th}} + 1)(2\hat{a}\hat{\rho}\hat{a}^\dagger + \hat{a}^\dagger\hat{a}\hat{\rho} + \hat{\rho}\hat{a}^\dagger\hat{a}) \\ & + \frac{\kappa_b}{2}(\bar{n}_{\text{th}} + 1)(2\hat{b}\hat{\rho}\hat{b}^\dagger + \hat{b}^\dagger\hat{b}\hat{\rho} + \hat{\rho}\hat{b}^\dagger\hat{b}) \\ & + \frac{\kappa_c}{2}(\bar{n}_{\text{th}} + 1)(2\hat{c}\hat{\rho}\hat{c}^\dagger + \hat{c}^\dagger\hat{c}\hat{\rho} + \hat{\rho}\hat{c}^\dagger\hat{c}) \\ & + \frac{\kappa_a}{2}\bar{n}_{\text{th}}(2\hat{a}^\dagger\hat{\rho}\hat{a} + \hat{a}\hat{a}^\dagger\hat{\rho} + \hat{\rho}\hat{a}\hat{a}^\dagger) \\ & + \frac{\kappa_b}{2}\bar{n}_{\text{th}}(2\hat{b}^\dagger\hat{\rho}\hat{b} + \hat{b}\hat{b}^\dagger\hat{\rho} + \hat{\rho}\hat{b}\hat{b}^\dagger) \\ & + \frac{\kappa_c}{2}\bar{n}_{\text{th}}(2\hat{c}^\dagger\hat{\rho}\hat{c} + \hat{c}\hat{c}^\dagger\hat{\rho} + \hat{\rho}\hat{c}\hat{c}^\dagger), \end{aligned} \quad (12)$$

where  $\kappa_a$ ,  $\kappa_b$ , and  $\kappa_c$  denote the decay rates of mode  $a$ , mode  $b$ , and mode  $c$ , respectively.  $\bar{n}_{\text{th}} = \{\exp[\hbar\omega/(\kappa_B T)] - 1\}^{-1}$  is the mean number of thermal photons,  $\kappa_B$  is the Boltzmann

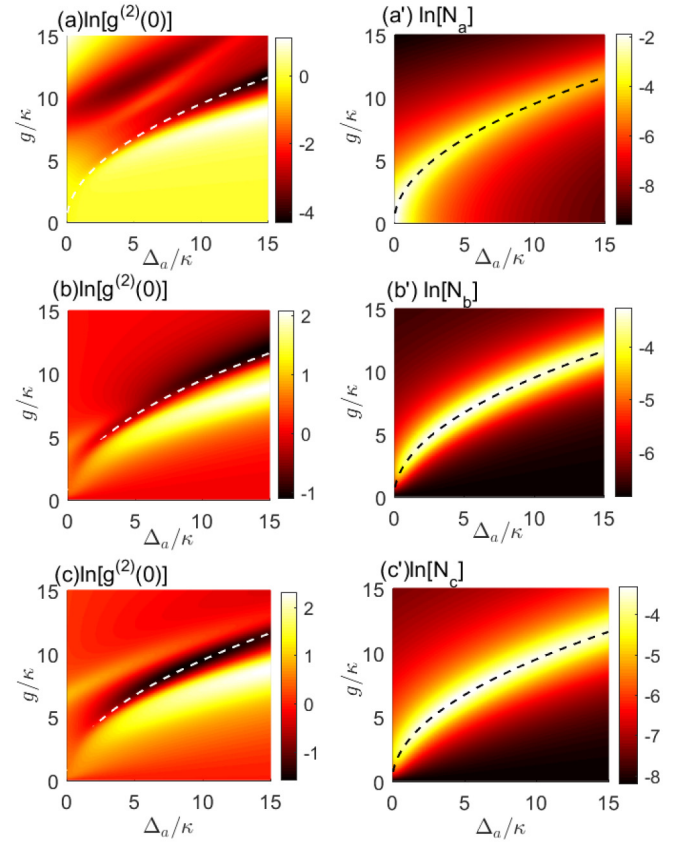


FIG. 2. The logarithmic plot (of base  $e$ ) of the zero-delay-time second-order correlation functions  $g^{(2)}(0)$  and average photon number  $N$  as a function of  $g/\kappa$  and  $\Delta_a/\kappa$  for mode  $a$ ,  $b$ , and  $c$ , respectively. (a, a') The statistical properties of mode  $a$ . (b, b') The statistical properties of mode  $b$ . (c, c') The statistical properties of mode  $c$ . The shared parameters are  $\Delta_b/\kappa = 3$ ,  $\Delta_c/\kappa = 6$ ,  $\bar{n}_{\text{th}} = 0$ ,  $\varepsilon_{la}/\kappa = 0.2$ , and  $\varepsilon_{lb}/\kappa = \varepsilon_{lc}/\kappa = 0.1$ . In all panels, the dotted line denotes the optimal conditions of the PB shown in Eq. (7).

constant, and  $T$  is the reservoir temperature at thermal equilibrium.

In this paper, we are concerned with the zero-delay-time second-order correlation function in the steady state, so we need the steady-state density operator  $\hat{\rho}_s$ , which can be obtained by setting  $\partial\hat{\rho}/\partial t = 0$ . The zero-delay-time second-order correlation function is defined by

$$g^{(2)}(0) = \frac{\langle \hat{j}^\dagger \hat{j}^\dagger \hat{j} \hat{j} \rangle}{\langle \hat{j}^\dagger \hat{j} \rangle^2}, \quad (13)$$

where  $j$  is selected from the modes  $a$ ,  $b$ , and  $c$ . When  $j = a$ , the second-order correlation function describes the statistical properties of photons in mode  $a$ . The second-order correlation function  $g^{(2)}(0) < 1$  corresponds to the sub-Poissonian statistics.

### B. Numerical results and comparison with the analytical conditions for the CPB

In this section, the numerical results are provided to study the CPB by plotting the second-order correlation function  $g^{(2)}(0)$  versus the system parameters, where  $g^{(2)}(0)$  can be

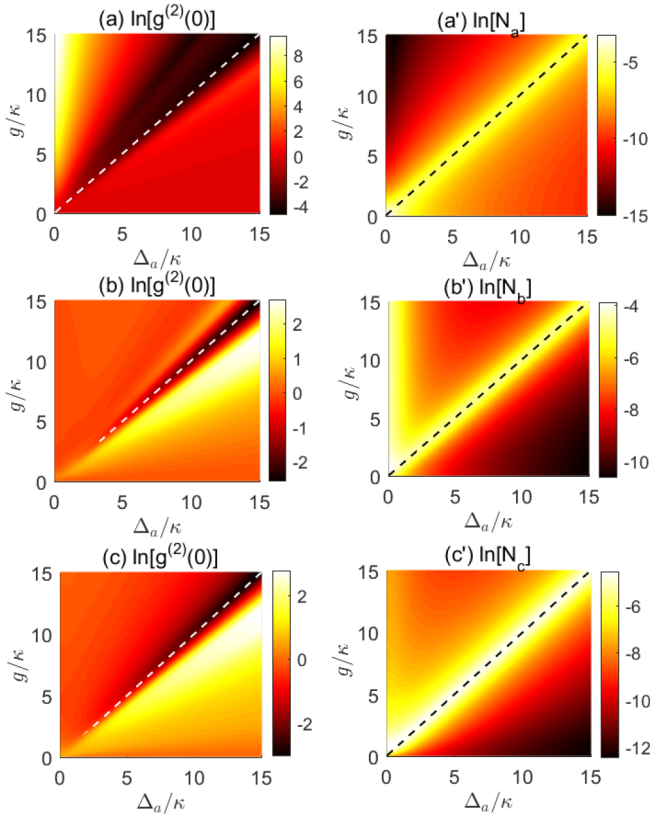


FIG. 3. The logarithmic plot of the zero-delay-time second-order correlation functions  $g^{(2)}(0)$  and average photon number  $N$  as a function of  $g/\kappa$  and  $\Delta_a/\kappa$  for mode  $a$ ,  $b$ , and  $c$ , respectively, where the condition  $\Delta_a = \Delta_b + \Delta_c$  is satisfied. The shared parameters are  $\bar{n}_{\text{th}} = 0$ ,  $\Delta_b = 2\Delta_a/3$ ,  $\Delta_c = \Delta_a/3$ ,  $\varepsilon_{la}/\kappa = 0.1$ ,  $\varepsilon_{lb}/\kappa = 0.05$ , and  $\varepsilon_{lc}/\kappa = 0.01$ . (a, a') The statistical properties of mode  $a$ . (b, b') The statistical properties of mode  $b$ . (c, c') The statistical properties of mode  $c$ . In all panels, the dotted line denotes the optimal conditions of the PB shown in Eq. (9).

obtained by substituting Hamiltonian  $\hat{H}_{\text{eff}}$  of Eq. (3) into the master equation of Eq. (12). The Hilbert spaces of the system are truncated to five dimensions for cavity modes  $a$ ,  $b$ , and  $c$ , respectively.

First, we numerically study the CPB effect under zero temperature ( $\bar{n}_{\text{th}} = 0$ ), and the results are compared with the analytic conditions for CPB shown in Eq. (7). Here, the decay rates of the cavity modes are assumed to be equal, i.e.,  $\kappa_a = \kappa_b = \kappa_c = \kappa$ . And we rescale all the parameters with respect to the decay rate  $\kappa$ . In Figs. 2(a), 2(b) and 2(c), we plot the logarithmic plot of zero-delay-time second-order correlation functions  $g^{(2)}(0)$  as a function of  $g/\kappa$  and  $\Delta_a/\kappa$  for mode  $a$ ,  $b$ , and  $c$ , respectively. The shared parameters are  $\Delta_b/\kappa = 3$ ,  $\Delta_c/\kappa = 6$ ,  $\varepsilon_{la}/\kappa = 0.2$ , and  $\varepsilon_{lb}/\kappa = \varepsilon_{lc}/\kappa = 0.1$ , where we have assumed continuous wave excitation in this paper. The numerical results show that the CPB can occur in the three modes simultaneously. The shape of the antibunching region looks like a quadratic function, where we only show the region with positive values of  $g/\kappa$ , because the region of  $g^{(2)}(0) < 1$  with a negative  $g/\kappa$  is symmetrical with the positive  $g$  about the horizontal axis. The analytic conditions shown in Eq. (7) are denoted by the dotted line,

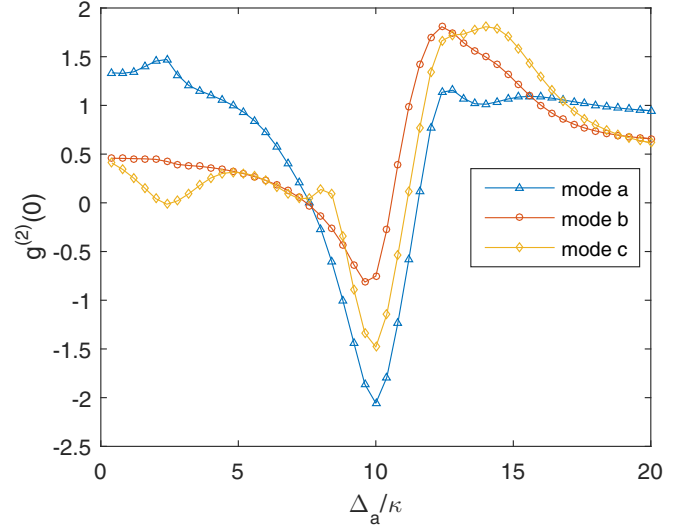


FIG. 4. The PB with nonzero temperature, where we plot the logarithmic plot of the zero-delay-time second-order correlation functions  $g^{(2)}(0)$  as a function of  $\Delta_a/\kappa$  under the optimal condition of Eq. (9) when  $\Delta_a = \Delta_b + \Delta_c$  is satisfied, where  $\Delta_b = 2\Delta_a/3$ ,  $\Delta_c = \Delta_a/3$ ,  $g/\kappa = 10$ ,  $\bar{n}_{\text{th}} = 0.001$ ,  $\varepsilon_{la}/\kappa = 0.2$ , and  $\varepsilon_{lb}/\kappa = \varepsilon_{lc}/\kappa = 0.1$ .

and are in agreement with numerical results. The brightness is defined as average photon number  $N = \langle \hat{a}^\dagger \hat{a} \rangle$ , which can be obtained by numerically solving the master equation. The brightness is plotted in Figs. 2(a'), 2(b'), and 2(c'). Comparing with Figs. 2(a), 2(b) and 2(c), the valleys with strong photon antibunching correspond to the large average photon numbers. Different from the other schemes of the CPB, the character of the three-wave-mixing system means that the photon antibunching can be realized in the three modes at the same time with different output frequencies.

In Fig. 3, we show the dependence of the second-order correlation functions  $g^{(2)}(0)$  on  $g$  and  $\Delta_a$  under the condition  $\Delta_a = \Delta_b + \Delta_c$ . The parameters are  $\Delta_b = 2\Delta_a/3$ ,  $\Delta_c = \Delta_a/3$ ,  $\varepsilon_{la}/\kappa = 0.1$ ,  $\varepsilon_{lb}/\kappa = 0.05$ , and  $\varepsilon_{lc}/\kappa = 0.01$ . We note that the strong photon antibunching (the dark region) appears exactly in the diagonal region for the three modes  $a$ ,  $b$ , and  $c$ , which are predicted by Eq. (9).

In the previous research, we study the CPB effect with zero temperature. Next, the CPB with nonzero temperature will be investigated. In Fig. 4, we plot zero-delay-time second-order correlation functions  $g^{(2)}(0)$  as a function of  $\Delta_a/\kappa$  for modes  $a$ ,  $b$ , and  $c$ , respectively, where  $\Delta_b = 2\Delta_a/3$ ,  $\Delta_c = \Delta_a/3$ ,  $g/\kappa = 10$ ,  $\bar{n}_{\text{th}}/\kappa = 0.001$ ,  $\varepsilon_{la}/\kappa = 0.2$ , and  $\varepsilon_{lb}/\kappa = \varepsilon_{lc}/\kappa = 0.1$ . The results show that the PB appears on  $\Delta_a/\kappa = 10$  for mode  $a$ , mode  $b$ , and mode  $c$ , just as predicted. The value of  $g^{(2)}(0)$  increases under nonzero temperature; however, the photon antibunching still exists, which indicates that the zero-temperature environment is not strictly required in this scheme.

The scheme is not restricted to a particular physical system. There are many potential physical systems to realize the three-wave-mixing-induced CPB. For example, a three-mode cavity filled with a high- $\chi^{(2)}$  nonlinear material [such as III-V semiconductors (e.g., GaAs, GaP, GaN, AlN, etc.) [44–46]] can realize the three-wave-mixing process,

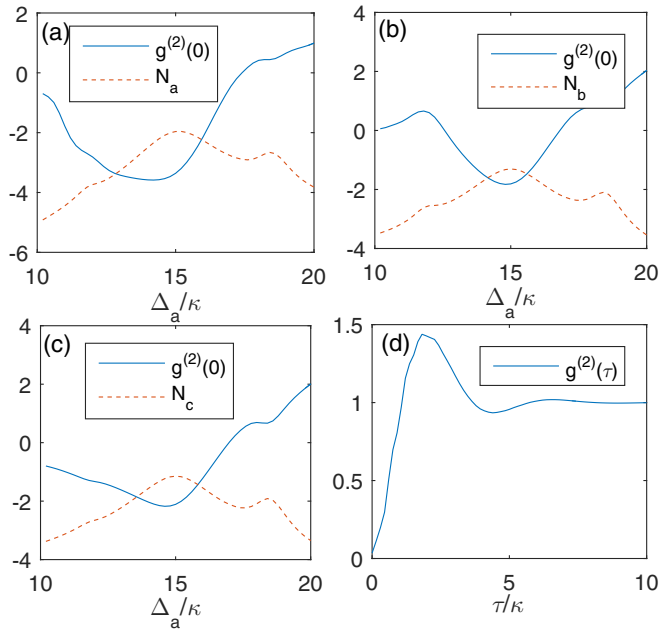


FIG. 5. (a, b, c) The logarithmic plot of the zero-delay-time second-order correlation functions and average photon number  $N$  as a function of  $\Delta_a$  for mode  $a$ ,  $b$ , and  $c$ , respectively, where the condition  $\Delta_a = \Delta_b + \Delta_c$  is satisfied. The shared parameters are  $\Delta_b = 4\Delta_a/5$ ,  $\Delta_c = \Delta_a/5$ ,  $\bar{n}_{th} = 0$ ,  $g = 15 \times 2\pi$  GHz,  $\kappa_a = 2\pi$  GHz,  $\kappa_b = 0.65 \times 2\pi$  GHz,  $\kappa_c = 0.54 \times 2\pi$  GHz,  $\varepsilon_{la} = 2\pi$  GHz,  $\varepsilon_{lb} = 0.4 \times 2\pi$  GHz, and  $\varepsilon_{lc} = 0.1 \times 2\pi$  GHz. (a)  $g^{(2)}(0)$  and  $N$  for mode  $a$ . (b)  $g^{(2)}(0)$  and  $N$  for mode  $b$ . (c)  $g^{(2)}(0)$  and  $N$  for mode  $c$ . (d)  $g^{(2)}(\tau)$  as a function of  $\tau$  for mode  $a$  with  $\Delta_a = g = 15 \times 2\pi$  GHz. The others parameters are the same as in panels (a), (b), and (c).

where bulk nonlinear susceptibility can be of the order of 10–200 pm/V in optoelectronics. A degenerate three-wave mixing  $g(\hat{a}\hat{b}^{\dagger 2} + \hat{b}^2\hat{a}^{\dagger})$  is proposed by a cyclic three-level artificial atom of a superconducting flux quantum circuit interacting with a two-mode superconducting transmission-line resonator [47], so the circuit QED is also a candidate to realize our scheme. In this paper, we adopt the experiment parameters of a triply resonant microring resonator with fabricated AlN microring structure [42]. The quality factor for mode  $a$  ( $b$ ,  $c$ ) is  $Q_a$  ( $Q_b$ ,  $Q_c$ ) =  $1.1 \times 10^5$  ( $1.8 \times 10^5$ ,  $2.6 \times 10^5$ ), and the corresponding decay rate is  $\kappa_a = 2\pi$  GHz ( $\kappa_b = 0.65 \times 2\pi$  GHz,  $\kappa_c = 0.54 \times 2\pi$  GHz). The above parameters are chosen from Ref. [42]. A realistic order-of-magnitude estimate for the three-wave-mixing coefficient is  $g = 15 \times 2\pi$  GHz, where  $g$  can be reduced at the cost of increasing  $g^{(2)}(0)$ . Under the present parameters, we plot  $g^{(2)}(0)$  and  $N$  as a function of  $\Delta_a$

for mode  $a$ ,  $b$ , and  $c$  shown in Fig. 5. The second-order correlation functions of the three modes can reach  $g^{(2)}(0) \simeq 0.034$  for mode  $a$ ,  $g^{(2)}(0) \simeq 0.16$  for mode  $b$ , and  $g^{(2)}(0) \simeq 0.12$  for mode  $c$ , and the corresponding average photon number can reach  $N_a \simeq 0.14$ ,  $N_b \simeq 0.27$ , and  $N_c \simeq 0.32$ . We use  $R$  to denote the repetition rates, which are calculated as  $R_a = 0.14 \times 2\pi$  GHz,  $R_b = 0.18 \times 2\pi$  GHz, and  $R_c = 0.17 \times 2\pi$  GHz. The photon blockade regions correspond to a large average photon number and repetition rate, so our scheme can act as a single-photon source. In addition to the zero-delay-time second-order correlation functions, quantum signatures can also be found in photon-intensity correlations with a finite-time delay. The second-order correlation functions  $g^{(2)}(\tau)$  are plotted in Fig. 5(d), and it is shown that the photon antibunching will be observed when time delay  $\tau$  changes on a large scale.

## V. CONCLUSION

We have investigated the CPB with three-wave mixing caused by level splitting, where the three-wave mixing mediates the conversion of a photon with high frequency into two photons with different low frequencies. We considered the situation that the three modes are driven simultaneously. By solving the master equation in the steady-state limit and computing the zero-delay-time second-order correlation function, strong photon antibunching can be obtained in the three modes simultaneously. We derived the optimal conditions for the photon antibunching by analyzing the eigenvalues of the system Hamiltonian, and the optimal conditions are compared with the numerical results. We found that they are in good agreement, which confirms the analytic conditions and our theory.

## ACKNOWLEDGMENTS

This work is supported by Key-Area Research and Development Program of Guangdong Province under Grant No. 2018B0303326001; the Jiangxi Education Department Fund under Grant No. GJJ180873; the National Natural Science Foundation of China under Grants No. 11965017, No. 11705025, No. 11804228, and No. 11774076; the Fundamental Research Funds for the Central Universities under Grants No. 2412019FZ044, No. 3132019181, and No. 2412017QD005; the Science Foundation of the Education Department of Jilin Province during the 13th Five Year Plan Period under Grant No. JJKH20190262KJ the NKRDP of China under Grant No. 2016YFA0301802; and the Jiangxi Natural Science Foundation under Grant No. 20192ACBL20051.

- [1] A. Majumdar, M. Bajcsy, A. Rundquist, and J. Vučković, *Phys. Rev. Lett.* **108**, 183601 (2012).
- [2] W. Zhang, Z. Y. Yu, Y. M. Liu, and Y. W. Peng, *Phys. Rev. A* **89**, 043832 (2014).
- [3] X. W. Xu and Y. Li, *Phys. Rev. A* **90**, 033809 (2014).
- [4] X. W. Xu and Y. Li, *J. Opt. B* **46**, 035502 (2013).
- [5] O. Kyriienko, I. A. Shelykh, and T. C. H. Liew, *Phys. Rev. A* **90**, 033807 (2014).
- [6] S. Ferretti, V. Savona, and D. Gerace, *New J. Phys.* **15**, 025012 (2013).
- [7] H. Flayac and V. Savona, *Phys. Rev. A* **88**, 033836 (2013).
- [8] X. W. Xu and Y. Li, *Phys. Rev. A* **90**, 043822 (2014).
- [9] H. Z. Shen, Y. H. Zhou, and X. X. Yi, *Phys. Rev. A* **91**, 063808 (2015).
- [10] D. Gerace and V. Savona, *Phys. Rev. A* **89**, 031803(R) (2014).

- [11] Y. H. Zhou, H. Z. Shen, and X. X. Yi, *Phys. Rev. A* **92**, 023838 (2015).
- [12] Y. H. Zhou, H. Z. Shen, X. Q. Shao, and X. X. Yi, *Opt. Express* **24**, 17332 (2016).
- [13] Y. H. Zhou, H. Z. Shen, X. Y. Zhang, and X. X. Yi, *Phys. Rev. A* **97**, 043819 (2018).
- [14] A. Imamoglu, H. Schmidt, G. Woods, and M. Deutsch, *Phys. Rev. Lett.* **79**, 1467 (1997).
- [15] H. Z. Shen, Y. H. Zhou, H. D. Liu, G. C. Wang, and X. X. Yi, *Opt. Express* **23**, 32835 (2015).
- [16] H. Z. Shen, S. Xu, Y. H. Zhou, G. Wang, and X. X. Yi, *J. Phys. B* **51**, 035503 (2018).
- [17] H. Z. Shen, C. Shang, Y. H. Zhou, and X. X. Yi, *Phys. Rev. A* **98**, 023856 (2018).
- [18] Y. Yan, Y. Cheng, S. Guan, D. Yu, and Z. Duan, *Opt. Lett.* **43**, 5086 (2018).
- [19] X. Liang, Z. Duan, Q. Guo, C. Liu, S. Guan, and Y. Ren, *Phys. Rev. A* **100**, 063834 (2019).
- [20] S. Guan, W. P. Bowen, C. Liu, and Z. Duan, *Europhys. Lett.* **119**, 58001 (2017).
- [21] K. M. Birnbaum, A. Boca, R. Miller, A. D. Boozer, T. E. Northup, and H. J. Kimble, *Nature (London)* **436**, 87 (2005).
- [22] T. C. H. Liew and V. Savona, *Phys. Rev. Lett.* **104**, 183601 (2010).
- [23] H. J. Carmichael, *Phys. Rev. Lett.* **55**, 2790 (1985).
- [24] M. Bamba, A. Imamoglu, I. Carusotto, and C. Ciuti, *Phys. Rev. A* **83**, 021802(R) (2011).
- [25] H. J. Snijders, J. A. Frey, J. Norman, H. Flayac, V. Savona, A. C. Gossard, J. E. Bowers, M. P. van Exter, D. Bouwmeester, and W. Löffler, *Phys. Rev. Lett.* **121**, 043601 (2018).
- [26] C. Vaneph, A. Morvan, G. Aiello, M. Féchant, M. Aprili, J. Gabelli, and J. Estève, *Phys. Rev. Lett.* **121**, 043602 (2018).
- [27] A. Faraon, I. Fushman, D. Englund, N. Stoltz, P. Petroff, and J. Vučković, *Nat. Phys.* **4**, 859 (2008).
- [28] A. J. Hoffman, S. J. Srinivasan, S. Schmidt, L. Spietz, J. Aumentado, H. E. Tureci, and A. A. Houck, *Phys. Rev. Lett.* **107**, 053602 (2011).
- [29] Y. X. Liu, X. W. Xu, A. Miranowicz, and F. Nori, *Phys. Rev. A* **89**, 043818 (2014).
- [30] L. Tian and H. J. Carmichael, *Phys. Rev. A* **46**, R6801 (1992).
- [31] M. J. Werner and A. Imamoglu, *Phys. Rev. A* **61**, 011801(R) (1999).
- [32] R. J. Brecha, P. R. Rice, and M. Xiao, *Phys. Rev. A* **59**, 2392 (1999).
- [33] P. Rabl, *Phys. Rev. Lett.* **107**, 063601 (2011).
- [34] A. Nunnenkamp, K. Børkje, and S. M. Girvin, *Phys. Rev. Lett.* **107**, 063602 (2011).
- [35] A. Majumdar and D. Gerace, *Phys. Rev. B* **87**, 235319 (2013).
- [36] H. Z. Shen, Y. H. Zhou, and X. X. Yi, *Phys. Rev. A* **90**, 023849 (2014).
- [37] D. E. Chang, A. S. Sorensen, E. A. Demler, and M. D. Lukin, *Nat. Phys.* **3**, 807 (2007).
- [38] D. Gerace, H. E. Tureci, A. Imamoglu, V. Giovannetti, and R. Fazio, *Nat. Phys.* **5**, 281 (2009).
- [39] S. L. Su, Y. Z. Tian, H. Z. Shen, H. P. Zang, E. J. Liang, and S. Zhang, *Phys. Rev. A* **96**, 042335 (2017).
- [40] S. L. Su, Y. Gao, E. J. Liang, and S. Zhang, *Phys. Rev. A* **95**, 022319 (2017).
- [41] S. L. Su, E. J. Liang, S. Zhang, J. J. Wen, L. L. Sun, Z. Jin, and A. D. Zhu, *Phys. Rev. A* **93**, 012306 (2016).
- [42] X. Guo, C. L. Zou, H. Jung, and H. X. Tang, *Phys. Rev. Lett.* **117**, 123902 (2016).
- [43] Y. H. Zhou, H. Z. Shen, X. Y. Luo, Y. Wang, F. Gao, and C. Y. Xin, *Phys. Rev. A* **96**, 063815 (2017).
- [44] A. Rodriguez, M. Soljacic, J. D. Joannopoulos, and S. G. Johnson, *Opt. Express* **15**, 7303 (2007).
- [45] Z.-F. Bi, A. W. Rodriguez, H. Hashemi, D. Duchesne, M. Loncar, K.-M. Wang, and S. G. Johnson, *Opt. Express* **20**, 7526 (2012).
- [46] P. S. Kuo, J. Bravo-Abad, and G. S. Solomon, *Nat. Commun.* **5**, 3109 (2014).
- [47] Z. H. Wang, C. P. Sun, and Y. Li, *Phys. Rev. A* **91**, 043801 (2015).